Monthly Notices
of the
ROYAL ASTRONOMICAL SOCIETY

MNRAS **492,** 3459–3464 (2020)
Advance Access publication 2020 January 17

doi:10.1093/mnras/staa089

Photometric characterization of multiple populations in star clusters: the impact of the first dredge-up

Maurizio Salaris,[1★] Chris Usher,[1] Silvia Martocchia,[1,2] Emanuele Dalessandro,[3] Nate Bastian,[1] Sara Saracino,[1] Santi Cassisi,[4,5] Ivan Cabrera-Ziri[6†] and Carmela Lardo[7]

[1]*Astrophysics Research Institute, Liverpool John Moores University, 146 Brownlow Hill, Liverpool L3 5RF, UK*
[2]*European Southern Observatory, Karl-Schwarzschild-Strasse 2, D-85748 Garching bei München, Germany*
[3]*INAF-Osservatorio di Astrofisica e Scienza dello Spazio di Bologna, Via Gobetti 93/3, I-40129 Bologna, Italy*
[4]*INAF-Osservatorio Astronomico d'Abruzzo, via M. Maggini, sn. I-64100 Teramo, Italy*
[5]*INFN-Sezione di Pisa, Largo Pontecorvo 3, I-56127 Pisa, Italy*
[6]*Harvard-Smithsonian Center for Astrophysics, 60 Garden Street, Cambridge, MA 02138, USA*
[7]*Laboratoire d'astrophysique, Ecole Polytechnique Fédérale de Lausanne (EPFL), Observatoire de Sauverny, CH-1290 Versoix, Switzerland*

Accepted 2020 January 5. Received 2019 December 30; in original form 2019 November 26

ABSTRACT

The existence of star-to-star light-element abundance variations (multiple populations, MPs) in massive Galactic and extragalactic star clusters older than about 2 Gyr is by now well established. Photometry of red giant branch (RGB) stars has been and still is instrumental in enabling the detection and characterization of cluster MPs, through the appropriate choices of filters, colours, and colour combinations that are mainly sensitive to N and – to a lesser degree – C stellar surface abundances. An important issue not yet properly addressed is that the translation of the observed widths of the cluster RGBs to abundance spreads must account for the effect of the first dredge-up on the surface chemical patterns, hence on the spectral energy distributions of stars belonging to the various MPs. We have filled this gap by studying theoretically the impact of the dredge-up on the predicted widths of RGBs in clusters hosting MPs. We find that for a given initial range of N abundances, the first dredge-up reduces the predicted RGB widths in N-sensitive filters compared to the case when its effect on the stellar spectral energy distributions is not accounted for. This reduction is a strong function of age and has also a dependence on metallicity. The net effect is an underestimate of the initial N-abundance ranges from RGB photometry if the first dredge-up is not accounted for in the modelling, and also the potential determination of spurious trends of N-abundance spreads with age.

Key words: convection – stars: abundances – Hertzsprung–Russell and colour–magnitude diagrams – galaxies: star clusters: general.

1 INTRODUCTION

During the last 10–15 yr both spectroscopic and photometric observations have definitely established that individual Galactic globular clusters (GCs) host multiple populations (MPs) of stars, characterized by C-N, O-Na (and also, but not always, Mg-Al) anti-correlations and He abundance spreads (see e.g. Gratton, Carretta & Bragaglia 2012; Milone et al. 2017, 2018; Bastian & Lardo 2018; Gratton et al. 2019). Scenarios for the origin of MPs (reviewed, e.g. by Renzini et al. 2015; Bastian & Lardo 2018) generally invoke more than one episode of star formation, envisaging that stars with CNONa (and He) abundance ratios similar to those observed in halo field stars are the first objects to form (P1 stars), while stars enriched in N and Na (and He) and depleted in C and O formed later (P2 stars). These P2 stars are supposed to form out of chemically processed material ejected by some class of massive P1 stars, usually denoted as polluters. To date, none of the proposed polluters can explain quantitatively the full ensemble of chemical patterns observed in individual GCs (Renzini et al. 2015; Bastian & Lardo 2018).

Photometric (see e.g. Larsen et al. 2014; Dalessandro et al. 2016; Gilligan et al. 2019; Lagioia et al. 2019; Nardiello et al. 2019, and references therein) and to a lesser extent spectroscopic (Mucciarelli et al. 2009) observations have also shown that MPs are not confined only to Galactic GCs, but are present also in

★ E-mail: m.salaris@ljmu.ac.uk
† Hubble Fellow.

old clusters of the Magellanic Clouds (MCs), Fornax and M31. Integrated spectroscopy of old extragalactic clusters in M31 also confirms the signature of MPs amongst old massive stellar clusters (see e.g. Schiavon et al. 2013).

A further recent development has seen the detection of MPs in resolved massive extragalactic clusters down to ages of ∼2 Gyr through spectroscopy (Hollyhead et al. 2017, 2019), and to a much larger extent photometry (see e.g. Niederhofer et al. 2017a,b; Martocchia et al. 2018, 2019; Lagioia et al. 2019; Milone et al. 2019; Nardiello et al. 2019, and references therein). Even more recently, Bastian et al. (2019) found a signature of MPs also in intermediate-age massive clusters belonging to the galaxy NGC 1316, from integrated spectroscopy. These new results are extremely important, for they clearly point to a connection between the formation of old GCs and much younger massive clusters.

As mentioned above, photometry plays a crucial role in the detection and characterization of MPs in resolved clusters. Several authors have shown, both empirically and theoretically (see e.g. Salaris et al. 2006; Marino et al. 2008; Yong et al. 2008; Sbordone et al. 2011; Cassisi et al. 2013; Dalessandro et al. 2016; Mucciarelli et al. 2016; Milone et al. 2017; Dalessandro et al. 2018; Salaris et al. 2019), that appropriate choices of filters, colours, and colour combinations (these latter usually denoted as *pseudocolours*) are sensitive to the abundance of mainly nitrogen (plus carbon and oxygen to a much lesser extent) in the atmospheres of the target stars, and can clearly detect the presence of MPs (see e.g. Monelli et al. 2013; Piotto et al. 2015; Milone et al. 2017; Niederhofer et al. 2017b; Salaris et al. 2019). Due to the distance of the targets, red giant branch (RGB) stars are typically observed for photometric (and also spectroscopic) MP detection.

By analysing results for a number of MC clusters covering a large range of ages (2–8 Gyr), Martocchia et al. (2018) and Martocchia et al. (2019, hereinafter M19) found in their sample a general trend between the measured width of a cluster RGB and the cluster age. They considered the pseudocolours $C_{F343N,\,F438W,\,F814W} \equiv (F343N - F438W) - (F438W - F814W)$ and $C_{F336W,\,F438W,\,F343N} \equiv (F336W - F438W) - (F438W - F343N)$ in the filter systems of the WFC3 and ACS (for $F814W$) cameras on board the *Hubble Space Telescope* (*HST*) – both sensitive to the abundance of N in the stellar spectra – and found that the RGB width shows a general increase with increasing age in their cluster sample. A natural explanation for this occurrence is that the N spread in these massive clusters increases with increasing cluster age.

However, there is an important additional phenomenon to consider when translating the observed RGB widths to N abundance spreads, which has been so far largely unexplored. The samples of cluster stars considered in M19 are distributed between the base of the RGB and approximately the RGB bump. This range covers almost the entire evolution through the first dredge-up (FDU – see e.g. Karakas & Lattanzio 2014; Salaris et al. 2015, and references therein) that starts on the subgiant branch and ends below the RGB bump level. During the FDU the surface N abundance increases compared to the initial value, and from basic stellar physics we expect this increase to depend on the initial nitrogen abundances. The variation of the surface abundances due to the FDU impacts the stellar spectral energy distributions, hence the predicted colours and pseudocolours sensitive to this element. The upshot is that the observed RGB widths in M19 are determined by a combination of the initial N spreads plus the effect of the dredge-up. This is true for any colour or pseudocolour sensitive to the surface N abundance in RGB stars, such as $C_{F275W,\,F336W,\,F438W} \equiv (F275W - F336W) - (F336W - F438W)$ (see e.g. Milone et al. 2017; Saracino et al. 2019), $C_{F336W,\,F343N,\,F438W} \equiv (F336W - F343N) - (F343N - F438W)$ (Zennaro et al. 2019), and $C_{F275W,\,F343N,\,F438W} \equiv (F275W - F343N) - (F343N - F438W)$ (Milone et al. 2019), devised to detect MPs in GCs and younger MC massive clusters by means of the so-called 'chromosome maps'.

In this paper, we explore this issue showing qualitatively, and in case of M19 results also quantitatively, the important role played by the FDU when translating to N abundance spreads the observed RGB widths in magnitude-pseudocolour diagrams and chromosome maps. Section 2 presents our theoretical calculations and the effect of the FDU on the surface abundances of MP stars, followed in Section 3 by an analysis of the impact of the FDU on the $C_{F275W,\,F336W,\,F438W}$, $C_{F336W,\,F343N,\,F438W}$, and $C_{F275W,\,F343N,\,F438W}$ pseudocolours used in the chromosome maps to disentangle cluster MPs, plus a quantitative estimate of the effect on the $C_{F343N,\,F438W,\,F814W}$ pseudocolour employed by M19. Conclusions follow in Section 4.

2 MODELS

We have employed the BaSTI isochrones (Pietrinferni et al. 2004) for two P1 solar scaled chemical compositions with [Fe/H] = −0.35 and [Fe/H] = −1.3, respectively, representative of the MC clusters studied by M19. We have also isochrones with the same stellar evolution code but for a reference N-enhanced P2 compositions with [C/Fe] = −0.28 [N/Fe] = +0.80 [O/Fe] = −0.28 (that keeps the CNO sum unchanged compared to the P1 metal distribution) and the same two [Fe/H] values. As discussed by Salaris et al. (2015) and Bertelli Motta et al. (2017), BaSTI models reproduce the general observed trends of post-FDU [C/N] ratios as a function of age, measured in field halo stars and a sample of open clusters of various ages.

Using the model RGB effective temperatures, surface gravity, and surface chemical abundances as inputs, we have calculated model atmospheres and synthetic spectral energy distributions as in Martocchia et al. (2017), employing the ATLAS12 (Kurucz 1970, 2005) and SYNTHE (Kurucz & Furenlid 1979; Kurucz & Avrett 1981) codes, respectively. From these spectral energy distributions, we have then computed bolometric corrections to transform the bolometric luminosities of the stellar models to magnitudes in the *HST* WFC3 and ACS filter systems.

All calculations show that at the end of the main sequence the outer convection zone engulfs increasingly deeper regions, dredging to the surface matter partially processed by H-burning in the core – the FDU. In this phase, the N abundance slowly increases (and the carbon abundance slowly decreases, but to a much smaller extent), until the maximum penetration of the convective envelope is reached. At this point, the inner convective boundary starts to retreat towards the surface, leaving behind a chemical discontinuity. This discontinuity is eventually crossed by the advancing (in mass) H-burning shell, causing the appearance of the RGB bump in the luminosity function of old stellar populations (see e.g. Cassisi & Salaris 2013). The change of surface nitrogen abundance (and carbon, while the oxygen abundance is essentially never altered in the age range investigated here) during the FDU depends on the mass of the star (hence the population age, see e.g. Salaris et al. 2015, and references therein), but also on the initial abundance pattern. The reason is that during the FDU the convective envelope reaches layers where the abundances of C and N attained the equilibrium values of the CN cycle during the main sequence. The equilibrium abundance of N is typically higher (and the C abundance lower) than the standard solar scaled (or α-enhanced) counterpart for a given

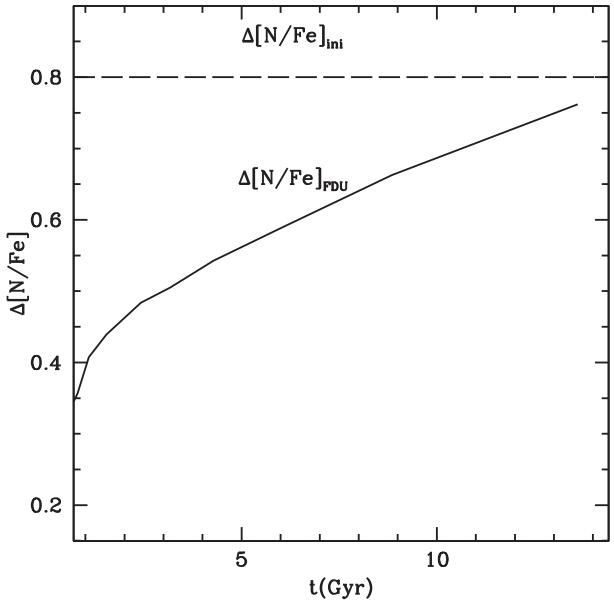

Figure 1. Initial value, $\Delta[\mathrm{N/Fe}]_{\mathrm{ini}} = 0.8$ (dashed line), of the difference in the surface [N/Fe] ratio for a set of bimodal populations with [Fe/H] = −1.3 and various ages *t*, and the corresponding difference $\Delta[\mathrm{N/Fe}]_{\mathrm{FDU}}$ in the surface abundances after the FDU (solid line, see the text for details).

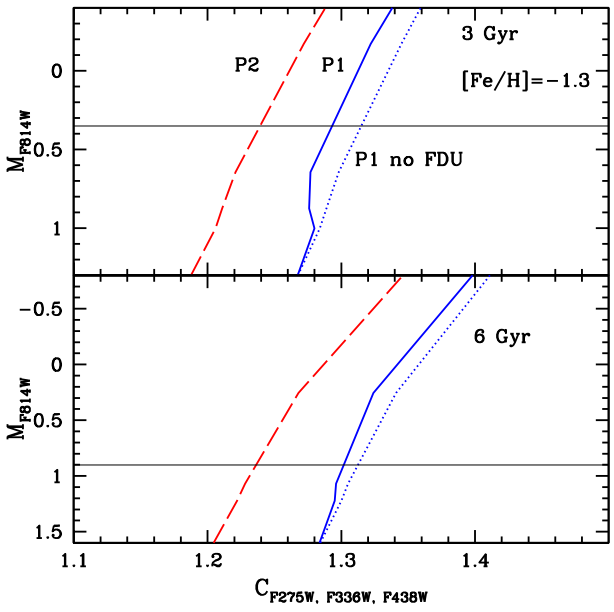

Figure 2. P1 (solid lines) and P2 (dashed lines) RGBs (at [Fe/H] = −1.30) in the $M_{F814W} - C_{F275W,\,F336W,\,F438W}$ diagram for ages equal to 3 (upper panel) and 6 (lower panel) Gyr, $\Delta[\mathrm{N/Fe}]_{\mathrm{ini}} = 0.8$, accounting for the effect of FDU on the spectral energy distributions. The dotted lines display P1 RGBs calculated without considering the variation of N (and C) due to the FDU. The horizontal thin lines mark the level corresponding to two magnitudes above the main-sequence turn-off, where the width of the RGB is taken in the chromosome maps (see the text for details).

total metallicity, hence the FDU causes an increase of surface N (and decrease of C). When the initial metal mixture is N-enhanced (and carbon depleted) the equilibrium abundance of N (and C) becomes more comparable to the initial one, and the effect of the FDU is much less appreciable or negligible.

Fig. 1 shows the run with age (ages between 1.0 and 13.5 Gyr) of Δ[N/Fe], defined as the difference of surface [N/Fe] between a population with N-enhanced P2 composition and a coeval one with P1 composition ([Fe/H] = −1.3 in this example) as inferred from our models. We show both the initial value $\Delta[\mathrm{N/Fe}]_{\mathrm{ini}}$ (the same for all ages) and the corresponding surface abundance differences at the completion of the FDU ($\Delta[\mathrm{N/Fe}]_{\mathrm{FDU}}$).

The values of $\Delta[\mathrm{N/Fe}]_{\mathrm{FDU}}$ are lower than $\Delta[\mathrm{N/Fe}]_{\mathrm{ini}}$, and display a clear trend with age, despite the fact that $\Delta[\mathrm{N/Fe}]_{\mathrm{ini}}$ is the same at all ages. For the younger populations, $\Delta[\mathrm{N/Fe}]_{\mathrm{FDU}}$ is much smaller than $\Delta[\mathrm{N/Fe}]_{\mathrm{ini}}$, but with increasing age it comes progressively closer to its initial value. The reason is that in RGB models with P1 initial N abundance, the surface [N/Fe] at the end of the FDU increases with decreasing age (see e.g. Salaris et al. 2015), while the impact of the FDU is much smaller or negligible in N-enhanced populations. The effect of the FDU on the surface carbon abundance is also small or negligible in P2 models with initial C-depleted abundances, while in P1 models the surface [C/Fe] at the end of the FDU gets progressively lower with decreasing age.

Summarizing, for bimodal coeval populations with fixed $\Delta[\mathrm{N/Fe}]_{\mathrm{ini}}$ (independent of age) and ages between 1.0 and 13.5 Gyr, the difference $\Delta[\mathrm{N/Fe}]_{\mathrm{FDU}}$ measured at the end of the FDU is predicted to be lower than the initial value, showing a trend with age – $\Delta[\mathrm{N/Fe}]_{\mathrm{FDU}}$ decreasing for decreasing age. This general behaviour is true irrespective of the exact value of [Fe/H].

3 ANALYSIS

We start here discussing the impact of the FDU on the representative N-sensitive $C_{F275W,\,F336W,\,F438W}$, $C_{F336W,\,F343N,\,F438W}$, and $C_{F275W,\,F343N,\,F438W}$ pseudocolours used in the chromosome maps to detect MPs from cluster photometry. In a chromosome map the total width of the cluster RGB in one of these pseudocolours is normalized to the value taken two magnitudes above the main-sequence turn-off in the *F*814*W* filter (Milone et al. 2017). This is a level where typically the FDU has either already started or is essentially completed, but still below the RGB bump, beyond which extra mixing processes that further affect the surface C and N abundances appear to be efficient, at least in low-mass stars (see e.g. Lagarde et al. 2019, and references therein).

As long as cluster ages are of the order of 10–13 Gyr, the effect of the FDU on the surface abundances – hence the RGB $C_{F275W,\,F336W,\,F438W}$, $C_{F336W,\,F343N,\,F438W}$, and $C_{F275W,\,F343N,\,F438W}$ values – is basically negligible, especially at low metallicity. The situation is however different for intermediate-age clusters, as shown in Figs 2–4, that display $M_{F814W} - C_{F275W,\,F336W,\,F438W}$, $M_{F814W} - C_{F336W,\,F343N,\,F438W}$, and $M_{F814W} - C_{F275W,\,F343N,\,F438W}$ diagrams for two P1–P2 bimodal populations (at a representative [Fe/H] = −1.3) with ages of 3 and 6 Gyr, respectively, including also P1 RGBs calculated without accounting for the FDU in the spectral energy distributions. In the case of the P2 models the FDU never changes appreciably the surface abundances. The level at which the total RGB width is normalized in the chromosome maps to compare different clusters (two magnitudes above the main-sequence turn-off in the *F*814*W* filter) is also marked.

At the beginning of the FDU the pseudocolour difference between P1 and P2 RGBs is essentially the same for these two ages, in all three diagrams; when moving to brighter magnitudes the FDU progresses, causing a reduced [N/Fe] (and [C/Fe]) difference between P1 and P2 stars at a given brightness, and a decreased separation of the sequences. The effect is stronger at younger ages because of the increasing impact of the FDU on the surface

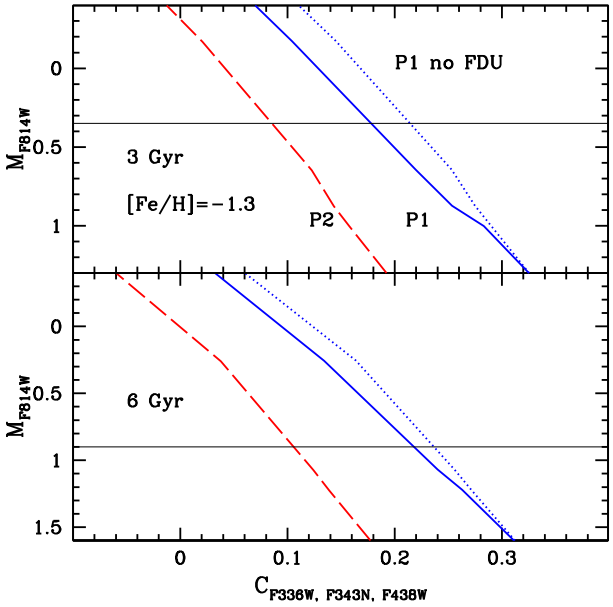

Figure 3. As Fig. 2 but for the $M_{F814W} - C_{F336W, F343N, F438W}$ diagram.

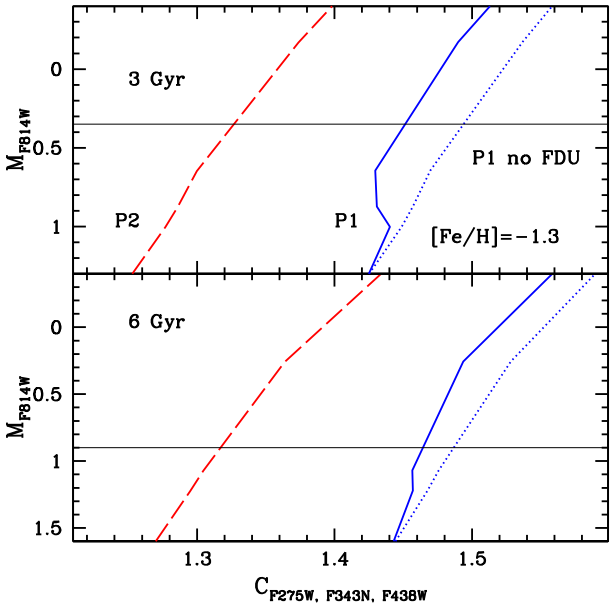

Figure 4. As Fig. 2 but for the $M_{F814W} - C_{F275W, F343N, F438W}$ diagram.

abundances (see Fig. 1). Clearly, any interpretation in terms of Δ[N/Fe]$_{ini}$ of the RGB widths in the chromosome maps must account for the effect of the FDU on the surface [N/Fe] and pseudocolours, for ages lower than typical GC ages.

To give at least one quantitative example of the role played by the FDU when inferring and/or comparing Δ[N/Fe]$_{ini}$ values amongst different clusters using N-sensitive photometric properties, we consider the $C_{F343N, F438W, F814W}$ pseudocolour employed by M19. Fig. 5 shows theoretical RGBs for two bimodal P1–P2 populations with ages equal to 6 and 13.5 Gyr at a representative [Fe/H] $= -1.3$ and Δ[N/Fe]$_{ini} = 0.8$, plotted in the $M_{F438W} - C_{F343N, F438W, F814W}$ diagram used by M19. The displayed range of M_{F438W} magnitudes corresponds approximately to the range employed in M19 analysis, which roughly encompasses the entire development of the FDU.

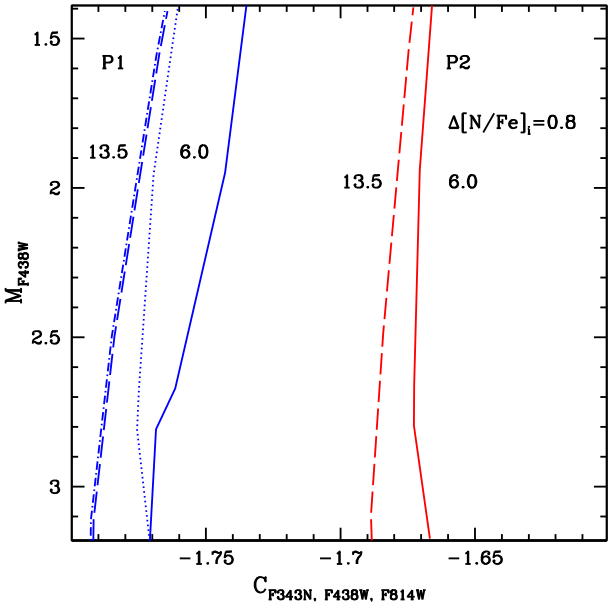

Figure 5. P1 and P2 RGBs (at [Fe/H] $= -1.30$) in the $M_{F438W} - C_{F343N, F438W, F814W}$ diagram for 6 (solid lines) and 13.5 (dashed lines) Gyr, Δ[N/Fe]$_{ini} = 0.8$, accounting for the FDU (that has a negligible effect on P2 RGBs). The dotted and dash–dotted blue lines display P1 RGBs calculated without considering the variation of N (and C) due to the FDU, for 6 and 13.5 Gyr, respectively (see the text for details).

As for the cases discussed before, at a given age, the $C_{F343N, F438W, F814W}$ separation between P1 and P2 RGBs decreases with decreasing magnitude, due to the effect of the FDU on the surface N abundances. The variation (decrease) of C plays a much smaller role, but has the same qualitative effect of the increase of N, which is to shift the RGB to larger values of $C_{F343N, F438W, F814W}$.

The dotted lines display the P1 RGBs that do not account for the effect of the FDU on the spectral energy distributions due to the change of the surface abundances. At 13.5 Gyr the no-FDU RGB is almost coincident with the FDU case, because at this metallicity and age its effect on the surface abundances is very small also for the P1 composition. For the 6 Gyr case, the no-FDU P1 RGB runs parallel to the P2 one, and diverges steadily from the calculations that include the FDU.

To assess quantitatively the impact of the FDU on the interpretation of M19 results, we have considered P1–P2 pairs of RGBs with Δ[N/Fe]$_{ini} = 0.8$, ages between 3 and 13.5 Gyr for [Fe/H] $= -1.3$, and between 1 and 6 Gyr for [Fe/H] $= -0.35$. We have distributed randomly 100 stars with a 1:1 ratio between P1 and P2 objects, along the isochrones' RGBs employing a Salpeter mass function – the choice of the mass function is not critical because of the extremely narrow mass range involved – in the M_{F438W} range of Fig. 5. We have then added to each synthetic star photometry a typical Gaussian photometric error taken from the artificial star tests, which is approximately the same for all stars of the cluster sample, in this representative magnitude range. The number of synthetic stars is roughly the same as the number of stars employed in M19 analysis. For each pair of P1–P2 stars, we have then calculated the $C_{F343N, F438W, F814W}$ distribution and determined the 1σ dispersion $\sigma(C_{F343N, F438W, F814W})^{RGB}$ – as in M19 – repeating the procedure 100 times to determine its average value.

The top panel of Fig. 6 displays our theoretical $\sigma(C_{F343N, F438W, F814W})^{RGB}$ as a function of age, together with

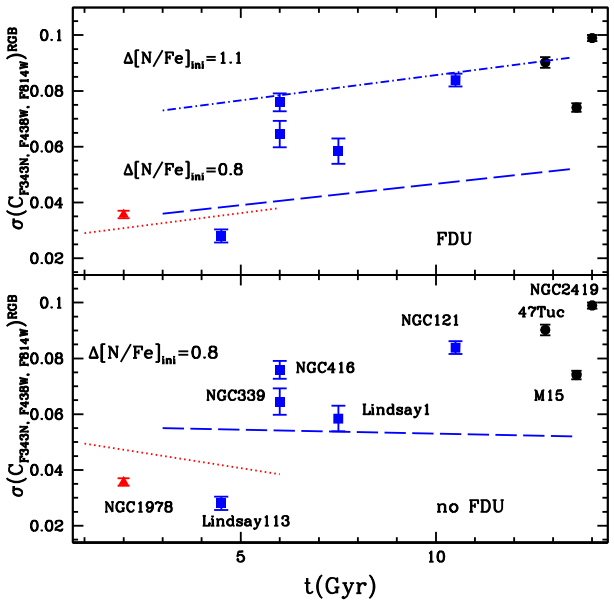

Figure 6. *Top panel:* Theoretical $\sigma(C_{F343N,\,F438W,\,F814W})^{RGB}$ as a function of age for [Fe/H] = −0.35 (dotted line), [Fe/H] = −1.3 (dashed line), and Δ[N/Fe]$_{ini}$ = 0.8. The dash–dotted line displays the results for Δ[N/Fe]$_{ini}$ = 1.1 and [Fe/H] = −1.3 (see the text for details). We also show the $\sigma(C_{F343N,\,F438W,\,F814W})^{RGB}$ values determined by M19 for a sample of MC clusters with photometric detection of MPs (filled red triangles for clusters with [Fe/H] around −0.35 and filled blue squares for clusters with [Fe/H] around −1.3). Results for three GCs are also displayed for comparison (filled black circles). *Bottom panel:* The same as the top panel but with theoretical $\sigma(C_{F343N,\,F438W,\,F814W})^{RGB}$ values calculated for Δ[N/Fe]$_{ini}$ = 0.8 without accounting for the effect of the FDU on the spectral energy distributions.

$\sigma(C_{F343N,\,F438W,\,F814W})^{RGB}$ measured by M19 for their sample of MC clusters that show MPs, plus M19 determinations for the Milky Way GCs 47 Tuc, M15, and NGC 2419. These bimodal MPs with 1:1 ratio and a constant Δ[N/Fe]$_{ini}$ = 0.8 display a trend with age qualitatively similar to the observations. This is due to the effect of the FDU on the surface N abundances discussed above. However, a constant Δ[N/Fe]$_{ini}$ with age does not match the observed average slope, for a linear fit to the observed $\sigma(C_{F343N,\,F438W,\,F814W})^{RGB}$ values gives a slope equal to 0.0060 ± 0.0005 mag Gyr^{-1}, while the theoretical results displayed in the figure have slopes equal to 0.0018 and 0.0015 mag Gyr^{-1} for [Fe/H] = −0.35 and [Fe/H] = −1.3, respectively. This implies that the observed trends are explained by a combination of both the effect of the FDU at constant Δ[N/Fe]$_{ini}$, and a general increase of Δ[N/Fe]$_{ini}$ with age.

To clarify this point, the same figure displays also the $\sigma(C_{F343N,\,F438W,\,F814W})^{RGB}$ values for the same type of bimodal MPs (1:1 ratio between P1 and P2 stars), but calculated considering P2 models with Δ[N/Fe]$_{ini}$ = 1.1 (and [C/Fe] = [O/Fe] = −1.0, to preserve the CNO sum). These values approximately match the upper envelope of the observed distribution, with Δ[N/Fe]$_{ini}$ = 1.1 that roughly agrees with the range measured spectroscopically in 47 Tuc (Carretta et al. 2005; Marino et al. 2016).

The theoretical $\sigma(C_{F343N,\,F438W,\,F814W})^{RGB}$ values at fixed age, [Fe/H], and Δ[N/Fe]$_{ini}$ depend of course on the statistical distribution of the [N/Fe] abundances within the prescribed range. Still considering a bimodal distribution in terms of [N/Fe], when changing the P1/P2 ratio from 1:1 to a population with 70 per cent P1 stars and 30 per cent P2 stars with Δ[N/Fe]$_{ini}$ either 0.8 or 1.1 dex, the $\sigma(C_{F343N,\,F438W,\,F814W})^{RGB}$ dispersions are reduced by only a few 0.001 mag. A larger reduction (by up to 0.03 mag in the case of Δ[N/Fe]$_{ini}$ = 1.1) is found when the [N/Fe] abundances are distributed uniformly within the prescribed Δ[N/Fe]$_{ini}$ range, a sort of extreme opposite case compared to a 1:1 bimodal [N/Fe] distribution. However, even in this case the increase of $\sigma(C_{F343N,\,F438W,\,F814W})^{RGB}$ with age is preserved. Equal-weight multiple subpopulations quantized in terms of [N/Fe] – depending on their number – lead to intermediate results between the bimodal 1:1 population, and the case of uniform [N/Fe] distribution.

The lower panel of Fig. 6 displays the theoretical $\sigma(C_{F343N,\,F438W,\,F814W})^{RGB}$ values for the same bimodal MPs calculated with Δ[N/Fe]$_{ini}$ = 0.8 and a 1:1 ratio between P1 and P2 stars, but without FDU. The absolute values and trends of $\sigma(C_{F343N,\,F438W,\,F814W})^{RGB}$ with age are different from the 'correct' ones that include the effect of the FDU. The $\sigma(C_{F343N,\,F438W,\,F814W})^{RGB}$ values are higher than the FDU case at the younger ages, showing a general anticorrelation with age. This of course impacts the determination of Δ[N/Fe]$_{ini}$ from the measured $\sigma(C_{F343N,\,F438W,\,F814W})^{RGB}$ values in a sample of clusters.

4 CONCLUSIONS

The impact of the FDU on the observed width of RGBs in old and intermediate-age clusters hosting MPs has been so far largely unexplored. We have addressed this issue by considering several N-sensitive pseudocolours employed to detect MPs in clusters of various ages. In all cases, for a given initial difference Δ[N/Fe]$_{ini}$ between coeval P1 and P2 populations, the effect of the FDU is to reduce the predicted RGB width compared to the case when the effect of the FDU on the spectral energy distribution is neglected. The reduction is a function of age, and has also some dependence on [Fe/H]. These effects stem from the dependence of the FDU variations of the surface N and, to a lesser degree, C abundances, on age and metallicity in models with P1 compositions.

In the specific case of the pseudocolour employed by M19, when the FDU is accounted for, a constant Δ[N/Fe]$_{ini}$ produces a general increase with age of the predicted $\sigma(C_{F343N,\,F438W,\,F814W})^{RGB}$, qualitatively similar to what is observed, but with a shallower slope. The observed trend with cluster age can be matched only by a combination of both the effect of the FDU at constant Δ[N/Fe]$_{ini}$, and a general increase of Δ[N/Fe]$_{ini}$ with age. When the theoretical spectral energy distributions do not account for the FDU, the values of Δ[N/Fe]$_{ini}$ required to match the observed RGB widths will be smaller. This effect only becomes significant for ages below ∼10 Gyr, when the FDU starts to alter more significantly the surface chemical composition – see e.g. the case of NGC 1978 in Fig. 6.

The FDU affects also the quantitative interpretation, in terms of N-abundance spreads, of the chromosome maps, when employed to identify MPs in intermediate-age clusters. In the case of GCs, due to their old ages, the FDU is largely unable to affect appreciably the surface N and C abundances, hence its effect on the $C_{F275W,\,F336W,\,F438W}$, $C_{F336W,\,F343N,\,F438W}$, or $C_{F275W,\,F343N,\,F438W}$ pseudocolours is negligible. At younger ages the FDU can affect the predicted values much more appreciably. Hence, also in case of the chromosome maps, neglecting the FDU abundance changes can lead to an underestimate of the initial [N/Fe] spread for a given measured value of the RGB width.

The surface chemical changes due to the FDU play therefore an important role in the interpretation of the observed width of RGBs in intermediate-age clusters. It needs to be properly accounted for when determining initial N-abundance spreads from photometry, and potential correlations with age or other cluster parameters.

ACKNOWLEDGEMENTS

CU, NB, and SM gratefully acknowledge financial support from the European Research Council (ERC-CoG-646928, Multi-Pop). NB also acknowledges financial support from the Royal Society (University Research Fellowship). Support for ICZ was provided by National Aeronautics and Space Administration (NASA) through Hubble Fellowship grant HST-HF2-51387.001-A awarded by the Space Telescope Science Institute, which is operated by the Association of Universities for Research in Astronomy, Inc., for NASA, under contract NAS5-26555. SC acknowledges support from Premiale INAF MITiC, from Istituto Nazionale di Fisica Nucleare (INFN) (Iniziativa specifica TAsP), and grant AYA2013-42781P from the Ministry of Economy and Competitiveness of Spain.

REFERENCES

Bastian N., Lardo C., 2018, ARA&A, 56, 83
Bastian N. et al., 2019, MNRAS, 489, L80
Bertelli Motta C., Salaris M., Pasquali A., Grebel E. K., 2017, MNRAS, 466, 2161
Carretta E., Gratton R. G., Lucatello S., Bragaglia A., Bonifacio P., 2005, A&A, 433, 597
Cassisi S., Salaris M., 2013, Old Stellar Populations: How to Study the Fossil Record of Galaxy Formation, Wiley - VCH, Weinheim, Germany
Cassisi S., Mucciarelli A., Pietrinferni A., Salaris M., Ferguson J., 2013, A&A, 554, A19
Dalessandro E., Lapenna E., Mucciarelli A., Origlia L., Ferraro F. R., Lanzoni B., 2016, ApJ, 829, 77
Dalessandro E. et al., 2018, A&A, 618, A131
Gilligan C. K. et al., 2019, MNRAS, 486, 5581
Gratton R. G., Carretta E., Bragaglia A., 2012, A&AR, 20, 50
Gratton R., Bragaglia A., Carretta E., D'Orazi V., Lucatello S., Sollima A., 2019, A&AR, 27, 8
Hollyhead K. et al., 2017, MNRAS, 465, L39
Hollyhead K. et al., 2019, MNRAS, 484, 4718
Karakas A. I., Lattanzio J. C., 2014, Publ. Astron. Soc. Aust., 31, e030
Kurucz R. L., 1970, SAO Special Report, 309
Kurucz R. L., 2005, Memorie della Societa Astronomica Italiana Supplementi, 8, 14
Kurucz R. L., Avrett E. H., 1981, SAO Special Report, 391
Kurucz R. L., Furenlid I., 1979, SAO Special Report, 387
Lagarde N. et al., 2019, A&A, 621, A24
Lagioia E. P., Milone A. P., Marino A. F., Dotter A., 2019, ApJ, 871, 140
Larsen S. S., Brodie J. P., Grundahl F., Strader J., 2014, ApJ, 797, 15
Marino A. F., Villanova S., Piotto G., Milone A. P., Momany Y., Bedin L. R., Medling A. M., 2008, A&A, 490, 625
Marino A. F. et al., 2016, MNRAS, 459, 610
Martocchia S. et al., 2017, MNRAS, 468, 3150
Martocchia S. et al., 2018, MNRAS, 473, 2688
Martocchia S. et al., 2019, MNRAS, 487, 5324 (M19)
Milone A. P. et al., 2017, MNRAS, 464, 3636
Milone A. P. et al., 2018, MNRAS, 481, 5098
Milone A. P. et al., 2020, MNRAS, 491, 515
Monelli M. et al., 2013, MNRAS, 431, 2126
Mucciarelli A., Origlia L., Ferraro F. R., Pancino E., 2009, ApJ, 695, L134
Mucciarelli A. et al., 2016, ApJ, 824, 73
Nardiello D., Piotto G., Milone A. P., Rich R. M., Cassisi S., Bedin L. R., Bellini A., Renzini A., 2019, MNRAS, 485, 3076
Niederhofer F. et al., 2017a, MNRAS, 464, 94
Niederhofer F. et al., 2017b, MNRAS, 465, 4159
Pietrinferni A., Cassisi S., Salaris M., Castelli F., 2004, ApJ, 612, 168
Piotto G. et al., 2015, AJ, 149, 91
Renzini A. et al., 2015, MNRAS, 454, 4197
Salaris M., Weiss A., Ferguson J. W., Fusilier D. J., 2006, ApJ, 645, 1131
Salaris M., Pietrinferni A., Piersimoni A. M., Cassisi S., 2015, A&A, 583, A87
Salaris M., Cassisi S., Mucciarelli A., Nardiello D., 2019, A&A, 629, A40
Saracino S. et al., 2019, MNRAS, 489, L97
Sbordone L., Salaris M., Weiss A., Cassisi S., 2011, A&A, 534, A9
Schiavon R. P., Caldwell N., Conroy C., Graves G. J., Strader J., MacArthur L. A., Courteau S., Harding P., 2013, ApJ, 776, L7
Yong D., Grundahl F., Johnson J. A., Asplund M., 2008, ApJ, 684, 1159
Zennaro M., Milone A. P., Marino A. F., Cordoni G., Lagioia E. P., Tailo M., 2019, MNRAS, 487, 3239

This paper has been typeset from a TEX/LATEX file prepared by the author.